



**HAL**  
open science

## Theranostic MRI liposomes for magnetic targeting and ultrasound triggered release of the antivascular CA4P

Caroline J Thébault, Grégory Ramniceanu, Sarah Boumati, Aude Michel, Johanne Seguin, Benoit Larrat, Nathalie Mignet, Christine Ménager, Bich-Thuy Doan

### ► To cite this version:

Caroline J Thébault, Grégory Ramniceanu, Sarah Boumati, Aude Michel, Johanne Seguin, et al..  
Theranostic MRI liposomes for magnetic targeting and ultrasound triggered release of the antivascular  
CA4P. *Journal of Controlled Release*, 2020, 322, pp.137-148. 10.1016/j.jconrel.2020.03.003 . hal-  
03059422

**HAL Id: hal-03059422**

**<https://hal.science/hal-03059422>**

Submitted on 4 May 2021

**HAL** is a multi-disciplinary open access archive for the deposit and dissemination of scientific research documents, whether they are published or not. The documents may come from teaching and research institutions in France or abroad, or from public or private research centers.

L'archive ouverte pluridisciplinaire **HAL**, est destinée au dépôt et à la diffusion de documents scientifiques de niveau recherche, publiés ou non, émanant des établissements d'enseignement et de recherche français ou étrangers, des laboratoires publics ou privés.

# Theranostic MRI liposomes for magnetic targeting and ultrasound triggered release of the antivasular CA4P

Caroline J. Thébault<sup>a, b, c</sup>, Grégory Ramniceanu<sup>a, b</sup>, Sarah Boumati<sup>a, b</sup>, Aude Michel<sup>e</sup>, Johanne Seguin<sup>b</sup>, Benoit Larrat<sup>d, e</sup>, Nathalie Mignet<sup>b</sup>, Christine Ménager<sup>c</sup>, Bich-Thuy Doan<sup>a, b</sup>.

a : Université PSL, Chimie ParisTech, CNRS, SEISAD, Unité de Technologies Chimiques et Biologiques pour la Santé (UTCBS), F-75005 Paris, France.

b : Université de Paris, UTCBS, CNRS, INSERM, Faculté de Pharmacie, 4 av de l'observatoire, F-75006 Paris, France, <http://www.cnrs.utcbs.fr/>

c : Sorbonne Université, CNRS, PHysico-chimie des Electrolytes et Nanosystèmes Interfaciaux, PHENIX, F-75005 Paris, France.

d : NeuroSpin, Institut des Sciences du Vivant Frédéric Joliot, Commissariat à l'Energie Atomique et aux Énergies Alternatives (CEA), F- 91191 Gif-sur-Yvette, France

e : Université Paris Saclay, F-91190 Saint-Aubin, France.

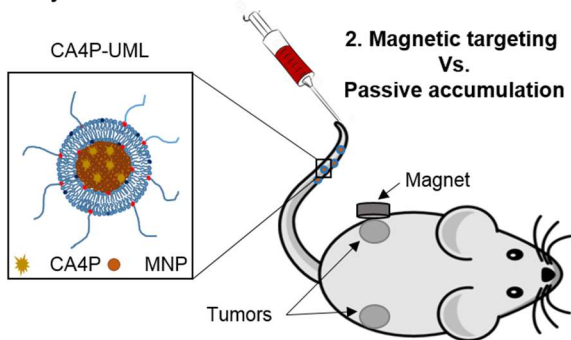
Corresponding author: Dr Bich-Thuy Doan, [bich-thuy.doan@chimieparistech.psl.eu](mailto:bich-thuy.doan@chimieparistech.psl.eu) and Pr Christine Ménager, [christine.menager@sorbonne-universite.fr](mailto:christine.menager@sorbonne-universite.fr)

## **Abstract**

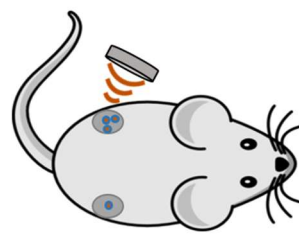
Theranostic nanocarriers of antivasular drug encapsulated in thermosensitive ultramagnetic liposomes can be advantageously designed to provide a locally high concentration and an active delivery, with image-guided Magnetic Resonance Imaging (MRI) so as to reliably cure tumor. We propose a novel therapeutic strategy consisting of the magnetic accumulation of Ultra Magnetic Liposomes (UML) followed by High-Intensity Focused Ultrasound (HIFU) to trigger the release of an antivasular agent monitored by MRI. For this purpose, we co-encapsulated Combretastatin A4 phosphate (CA4P), a vascular disrupting agent, in the core of UML to obtain CA4P-loaded thermosensitive UltraMagnetic Liposomes (CA4P-UML). To assess the HIFU parameters, the CA4P release has been triggered *in vitro* by local heating HIFU at the lipids transition temperature. Morphology of endothelial cells was assessed to evaluate the effect of encapsulated versus non-encapsulated CA4P. The efficiency of a treatment combining the magnetic targeting of CA4P-UML with the CA4P release triggered by HIFU was studied in CT26 murine tumors. Tumor perfusion and volume regression parameters were monitored by multiparametric quantitative anatomical and dynamic *in vivo* MRI at 7 T. Additionally, vascularization and cellularity were evaluated *ex-vivo* by histology. This thorough investigation showed that the combined treatment exhibited a full benefit. A 150-fold improvement compared with the chemotherapy alone was obtained using a magnetic targeting of CA4P-UML triggered by HIFU, and was consistent with an expected effect on vascularization 24 h after treatment.

**Graphical abstract:**

**1. Injection of CA4P-UML**

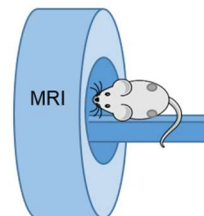


**2. Magnetic targeting  
Vs.  
Passive accumulation**



**3. HIFU-triggered CA4P release  
Vs.  
Passive release**

**4. Treatment efficiency  
monitored by MRI**



**Keywords:** *Antivascular therapy, ultramagnetic liposomes, Magnetic Resonance Imaging, High Intensity Focused Ultrasound, Magnetic nanoparticles.*

## Introduction

Combretastatin A4 phosphate (CA4P) is a water-soluble pro-drug of the Combretastatin A4 (CA4), a vascular disrupting agent (VDA). In cells, the link of CA4 with tubulin prevents the polymerization of microtubules that are essential for the cytoskeleton formation and cell division [1]. Treatment with CA4 results in the rounding up and blebbing of the endothelial cells which induces a rapid shutdown of the tumor vascular system [2]. VDAs advantageously bind to the immature and unstable tumor vasculature rather than to the normal one [3]. CA4P is currently under phase II clinical trial for non-squamous non-small-cell lung cancer, thyroid, ovarian, tubal and peritoneal carcinoma [4–6]. However, cardiovascular adverse effects were observed in patients after the administration of CA4P [7]. These toxicities could be bypassed with the use of targeted nanotechnologies in order to improve the accumulation of the drug at the tumor site.

The development of nanocarriers encapsulating chemotherapeutic drugs enables the reduction of their toxicity in healthy organs by increasing the targeting of the tumor. CA4P was already vectorized in smart nanocarriers such as nanogels, micelles, or liposomes [8-10]. As an example, a dual-drug delivery system based on nanogel-incorporated injectable hydrogel showed sequential release CA4P and Doxorubicin (DOX) and exhibited high inhibitory activities on cancer cell proliferation *in vitro*. With pH-responsive features, the carrier displayed superior therapeutic efficacy *in vivo* [8]. Reverse micelles-in-microspheres have also been reported showing a sustained release of water-soluble combretastatin A4 phosphate for S180 tumor treatment [9].

However, the passive accumulation of these nanocarriers on the tumor site strongly depends on the physicochemical properties of the carrier but also on the vascularization of the tumor. Hence, targeting strategies were developed in order to enhance the amount of drug delivered to the tumor site. For instance, immunoliposomes composed of CA4P coated with E-Selectin combined with irradiation resulted in a significant impact in tumor growth delay in mice as compared to free CA4P or targeted liposomes alone [10]. Magnetic targeting strategies were also successfully developed for many carriers. Among them, magnetic liposomes, also called Ultra Magnetic Liposomes (UML) because they contain a volume ratio of magnetic nanoparticles, have been developed [12]. Due to their magnetic charge which was previously determined by magnetization measurements around 20% in volume fraction, UML have shown the ability to be accumulated in xenografted murine colon tumors with a factor 3 increase as regard to non-targeted liposomes [11]. Despite the presence of magnetic nanoparticles there is enough free space to expect a high loading of CA4P in the aqueous part of the liposomes. Considering the magnetic relaxivities for MRI, encapsulation of magnetic nanoparticles in ULM provides cooperating MNP and gives a higher magnetic moment, resulting in a higher proton spin dephasing with shortened  $T_2$  value [11] allows to multiply by a factor of 3 the  $r_2$  relaxivity and by a factor of 5 the  $r_2:r_1$  ratio, leading to a far more efficient contrast agent for MRI.

Another interest of magnetic nanocarriers, is the possibility to trigger the release in a controlled manner. One strategy could be to use the heat generated by the magnetic particles under alternative magnetic field. For example, alternative magnetic field AMF was able to heat magnetic nanoparticles and release by thermosensitive effect encapsulated active [13–15]. However, one big issue of magnetic hyperthermia is the global heat generated as the magnetic field is not focused. Therefore, it is difficult to avoid undesirable heating of organs such as the liver in which the particles have mostly accumulated.

Hybrid MRI-HIFU is now available in clinic and could provide an easy way to trigger the release of drugs from nanocarriers under MRI guidance. Focused Ultrasound has been regarded as a very powerful method because it can allow an increase of the accumulation of the

nanocarriers in the tumors due to a permeabilization of vascular walls and also a triggered drug release due to ultrasound induced hyperthermia. Thermosensitive formulations of liposomes were developed to this end.

Here, we propose to encapsulate the CA4P in ultramagnetic liposomes (CA4P-UML) and control its release with HIFU, moreover *in vivo* MRI methods will be used to assess the efficiency of the therapy. CA4P-UML consists of Magnetic Nanoparticles (MNP) of maghemite ( $\gamma\text{-Fe}_2\text{O}_3$ ) and CA4P both encapsulated in the aqueous core of a thermosensitive liposome. After the magnetic targeting of CA4P-UML in the tumor, HIFU was used to locally increase the temperature to reach the lipid transition temperature and to trigger the CA4P release (Figure 1). To monitor the efficiency of the treatment, tumor volume and perfusion were studied by multiparametric *in vivo* MRI, allowing a non-invasive longitudinal quantitation in time of the tumor behaviour. VDAs are indeed expected to destroy the microvascularisation which would impact the blood perfusion and kill the tumor cells. The tumor was also analyzed by histology to comprehend the cellular impact of the treatment.

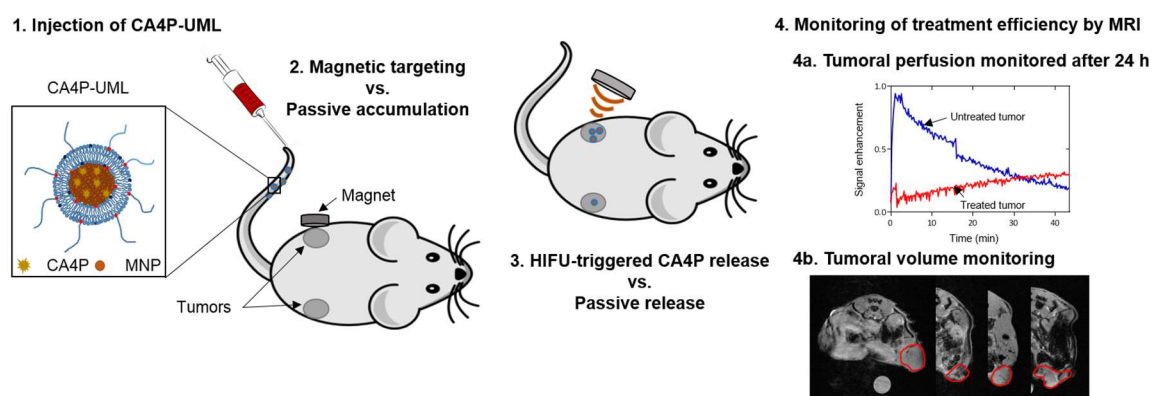


**Figure 1.** Schematic representation of the CA4P-UML treatment with magnetic targeting, HIFU drug release, and MRI monitoring.

## Materials & Methods

### 1. Materials

1,2-dipalmitoyl-sn-glycero-3-phosphocholine (DPPC), 1,2-distearoyl-sn-glycero-3-phosphocholine (DSPC) and 1,2-distearoyl-sn-glycero-3-phosphoethanolamine-N-[amino(polyethylene glycol)-2000] (ammonium salt) (DSPE-PEG2000) were purchased from Avanti Polar lipids, Inc. The CT26 murine colon carcinoma cell line (ATCC, CRL-2638) and the EA.hy926 human endothelial cell line (ATCC, CRL-2922) were purchased from American Type Culture Collection (LGC Standards, Molsheim, France). RPMI 1640 and DMEM culture medium, fetal bovine serum, Trypsine-EDTA and Streptomycin were purchased from Gibco Life Technologies. Combretastatin A-4 Phosphate (CA4P) was purchased from Toroma Organics (Saarbrücken, Germany).

### 2. Synthesis

Magnetic Nanoparticles (MNP) of maghemite ( $\gamma\text{-Fe}_2\text{O}_3$ ) with a mean diameter  $d_0$  of 9.8 nm and a polydispersity of 0.37 (S1) were synthesized by a co-precipitation method according to the

Massart process [16] and stabilized with citrate molecules at pH 7 [17,18]. UML were prepared as described in our previous work by a reverse-phase evaporation method [12]. To synthesize CA4P-UML, solutions of 1,2-dipalmitoyl-*sn*-glycero-3-phosphocholine (DPPC), 1,2-distearoyl-*sn*-glycero-3-phosphocholine (DSPC) and 1,2-distearoyl-*sn*-glycero-3-phosphoethanolamine-N-[amino(polyethylene glycol)-2000] (ammonium salt) (DSPE-PEG<sub>2000</sub>) were prepared respectively, 10 mg/mL, 10 mg/mL and 25 mg/mL in chloroform. MNP was dispersed at 2 M of iron in injection buffer (0.11 M NaCl, 0.02 M sodium citrate and 0.01 M HEPES) and CA4P was diluted at 12 mg/mL in the same buffer. These solutions were then mixed to obtain 1 mL of an aqueous phase with an iron concentration of 1 M and a CA4P concentration of 6 mg/mL. Phospholipids were solubilized in chloroform and diethyl ether (1/3, v/v) with a DPPC/DSPC/DSPE-PEG<sub>2000</sub> molar ratio of 86/9/5 and 1 mL of the aqueous phase were added. A water-in-oil emulsion was obtained by sonication for 20 min in an ultrasound bath and organic solvent was evaporated using a rotavapor. After filtration with a 0.45 µm syringe filter, CA4P-UML were dispersed in injection buffer (0.11 M NaCl, 0.02 M sodium citrate and 0.01 M HEPES). Non-encapsulated MNP and CA4P were eliminated by two magnetic sortings with a strong NdFeB magnet (150 x 100 x 25 mm, Supermagnete, Germany) [12].

### 3. Physico-chemical characterization

To visualize CA4P-UML, a carbon, copper grid was submerged in CA4P-UML solution at 1 mM iron and was allowed to dry. Transmission Electron Microscopy was then performed on a JEOL 100CX Transmission Electronic at 100 keV (IMPC-FR2482 platform).

The diameters of CA4P-UML were measured by Tunable Resistive Pulse Sensing (TRPS) using a qNano system (Izon Science, Oxford, UK) and data acquired with Izon Control Suite software V3.1. CA4P-UML were diluted 1000 times in injection buffer and passed through a nanopore NP200 with 5 bars pressure. To determine the size and concentration of the objects, calibration particles (CPC200B, Izon Science, Oxford, UK) with known diameter were used. Iron was quantified by Atomic Absorption Spectroscopy (AAS) after degradation of UML in 37% HCl.

The amount of CA4P encapsulated into UML was measured by the titration of non-encapsulated CA4P from the two supernatants of the magnetic sorting. Three ultrafiltration cycles were conducted on Nanosep<sup>®</sup> 10 kD at 3000 rpm for 20 min on a MiniSpin centrifuge (Eppendorf) to separate non-encapsulated CA4P from non-encapsulated MNP. CA4P was then titrated by absorbance at 300 nm from a calibration curve established previously in injection buffer.

### 4. *In vitro* passive and triggered drug release study

To assess passive drug release from CA4P-UML at physiological temperature, CA4P-UML were diluted at 110 µM of CA4P (corresponding to an iron concentration of 52 mM) in injection buffer (0.11 M NaCl, 0.02 M sodium citrate and 0.01 M HEPES). Liposome suspensions were placed in a water bath at 37°C and sampled after 0, 30, 45 and 60 min respectively. In each sample, released CA4P was separated from liposomes by three ultrafiltration cycles as explained previously and the absorbance was measured at 300 nm. The experiment was repeated 3 times.

The passive drug release was compared to an active drug release triggered by a temperature increase induced by HIFU. In order to do so, liposome suspensions contained in the tubes were first placed into a water bath at 37°C. After 30 min, they were quickly removed from the water bath and placed into a 6-well plate above a heating pad to maintain the temperature of the suspensions at 37°C. They were then sonicated by two consecutive HIFU sequences as detailed

in Table 1. The sonication started 30 min after putting the UML at 37°C so as to possibly get close to the *in vivo* protocol. Ultrasound was shot by a single element spherically focused transducer (diameter 25 mm, focal depth 20 mm, Imasonic, France) operating at 1.5 MHz. A dedicated programmable radiofrequency generator and amplifier (Image-Guided Therapy, France) were used to feed the transducer. The active piezoelectric surface was coupled to the liquid medium through a balloon filled with degassed water and closed by a latex membrane. The focal spot size (full width half maximum) was previously measured at 1.2x1.2x6.2 mm<sup>3</sup>. The samples were gently stirred during HIFU in order to homogenize the temperature within the sample. This heating protocol was first developed empirically in order to increase the temperature of a 10 mL solution from 37°C to 43°C ± 0.7 °C (Sequence 1) and then to maintain it roughly constant for 5 min (Sequence 2). This heating time course was validated using an electronic thermometer.

**Table 1.** Description of consecutive HIFU sequences used for *in vitro* studies.

|            | <b>Peak negative acoustic pressure at focus</b> | <b>Pulse duration</b> | <b>Delay</b> | <b>Repetition</b> |
|------------|---|-----------------------|--------------|-------------------|
| Sequence 1 | 1.7 MPa   | 120 s                 | -            | -                 |
| Sequence 2 | 1.3 MPa   | 5 s                   | 25 s         | 10                |

After exposure to HIFU, CA4P-UML suspensions were immediately placed back into the 37°C water bath. The suspensions were sampled at the same times as for the previously described passive release studies and the concentration of CA4P was measured by the same method.

## 5. Endothelial cell morphology

To assess the effect of CA4P-UML on the morphology of endothelial cells, an EA.hy926 cell line was used [19].

Cells were seeded in 24-well plates at a concentration of 15,000 cells/well in 500 µL of culture medium and incubated for 24 h at 37°C in a 5% CO<sub>2</sub>-humified atmosphere. Then, the medium was replaced by the UML, CA4P or CA4P-UML in a mixture of injection buffer and culture medium in a volumetric ratio of 1/5. Cells from two wells per condition were incubated with 200 µL of UML at 5 mM of iron, CA4P at 10 µM or CA4P-UML at 5 mM of iron and 10 µM of CA4P. The mixture of injection buffer and culture medium were used as control.

After a 5 h incubation, representative pictures of the cells were acquired with an x360 magnification microscope and cell circularities were measured using the software ImageJ [20]. The circularity is a shape descriptor used to compare cell morphology and defined as:

$$Circularity = 4\pi \frac{Area}{Perimeter^2}$$

The parametric student test was used to compare the means of groups two by two with a high number of samples [21].

## 6. Animals

Studies were carried out at 7 weeks old Balb/C female mice (Janvier, St Genest de Lisle, France). Animal experiments were conducted according to European and national guidelines and were approved by the institutional ethics committee (APAFiS # 7610).

## 7. Ectopic tumor implantation

A mouse bearing a subcutaneous CT26 tumor was sacrificed 14 days after implantation; following the removal, the tumor was submerged in DMEM culture medium and cut in 30 mm<sup>3</sup> fragments. Alcohol was used to disinfect the mouse flanks and the tumor fragments were transferred into sterile PBS and inserted subcutaneously using a 12 gauge trocar into the two mouse flanks[22].

CT26 was chosen according to a screening previously performed by our group to select the tumors according to their vascularization and marker expression [23]. Various imaging modalities have also been used to characterize this model [22]. Finally, the effect of CA4P on this model has been shown prior this study by Magnetic Resonance [24] and ultrasound imaging [25].

## 8. Experimental treatment protocol

The different groups of mice are described in Table 2. Mice were anesthetized with gaseous isoflurane at 1.5% in an air/O<sub>2</sub> mixture at 0.5 L/min and 0.2 L/min respectively.

**Table 2.** Mice treatment groups with n the number of tumors per condition.

|         | Injection   | Right tumor                   | Left tumor                           |
|---------|---|-------------------------------|--------------------------------------|
| Group A | -   | <b>Control</b><br>n = 8       | <b>HIFU</b><br>n = 8                 |
| Group B | CA4P-UML, intravenous injection (0.65 mg/kg of CA4P and 41 mg/kg of iron) | <b>CA4P-UML + MT</b><br>n = 7 | <b>CA4P-UML + HIFU</b><br>n = 7      |
| Group C | CA4P-UML, intravenous injection (0.65 mg/kg of CA4P and 41 mg/kg of iron) | <b>CA4P-UML</b><br>n = 9      | <b>CA4P-UML + MT + HIFU</b><br>n = 9 |
| Group D | CA4P by intravenous injection (0.65 mg/kg)                                | <b>CA4P IV</b><br>n = 6       |                                      |
| Group E | CA4P by intraperitoneal injection (100 mg/kg)                             | <b>CA4P IP x150</b><br>n = 3  |                                      |
| Group F | UML CA4P free, intravenous injection (41 mg/kg of iron)                   | <b>UML</b><br>n = 3           | <b>UML + MT + HIFU</b><br>n = 3      |

Ten days after tumor implantation, the treatment was injected by intraperitoneal injection for group E or by a catheter (30 G) placed in the caudal vein for groups B, C, D and F. For magnetic targeting (groups B, C and F), two cylindrical magnets (NdFeB, with diameter 6 mm x 2 mm thickness, 0.35 T at the magnet surface, Supermagnete, Germany) were stuck together and positioned on the skin over the tumor before the injection. Mice were kept in this position for 30 min. Then, the magnets were removed and two consecutive HIFU sequences described in Table 3 were applied to the left tumor for groups A, B, C and F. This heating protocol was set up in order to reach about 43°C *in vivo* and then to stabilize the temperature for 10 min. Two additional tumor bearing mice were used to develop this protocol under MR thermometry as detailed in supplementary information (S4)[26,27]. Body temperature was monitored during the whole procedure. Mice were placed on a heating blanket in order to maintain their body temperature at 37°C.

**Table 3.** Description of the consecutive HIFU sequences used for *in vivo* studies.

|            | <b>Peak acoustic pressure at focus</b> | <b>negative pressure</b> | <b>Pulse duration</b> | <b>Delay</b> | <b>Repetition</b> |
|------------|--|--------------------------|-----------------------|--------------|-------------------|
| Sequence 1 | 1.2 MPa                                |                          | 30 s                  | -            | -                 |
| Sequence 2 | 1.2 MPa                                |                          | 100 ms                | 100 ms       | 3 000             |

### 9. *In vivo* MRI assessment of anti-tumor efficacy

MRI provides quantitative imaging biomarkers that are efficient to assess anti-tumor therapy *in vivo*.

**MRI acquisitions:** MRI acquisitions were performed on a 7 T vertical spectrometer fitted with an ultra-shielded refrigerated magnet (300WB, Bruker, Avance II, Wissembourg, France), and equipped with an RF birdcage coil with a 40 mm inner diameter (Bruker) and a nominative 200 mT.m<sup>-1</sup> actively shielded gradient coil. Mice were anesthetized with gaseous isoflurane at 1.5% in an air/O<sub>2</sub> mixture at 0.5 L/min and 0.2 L/min respectively. Respiration rate was monitored during the whole procedure as well as the temperature in the cradle.

To monitor the tumor volume and the iron oxide targeting from the 25% percentile ratio %I<sub>0.25</sub>, [11], T<sub>2</sub>\*-weighted MRI images were acquired the day of treatment and 1, 4 and 7 days after treatment: FLASH images: Hermitian pulse, TR/TE = 350/5 ms, flip angle of 40°, triggered on respiration. A field of view of 3 x 3 cm<sup>2</sup>, a matrix size of 256 x 256 corresponding to 177 μm x 117 μm in plane resolution and 15 to 17 slices with a thickness of 1 mm were used, for an acquisition time of about 7 min.

A T<sub>1</sub>+T<sub>2</sub> mapping of the tumor was obtained 24 h after treatment by a RAREVTR sequence: Hermitian pulse, flip angle of 90° (+ 180°), TE = 11/22/33/44/55/66/88 ms, TR = 5/2/1.2/0.8/0.6/0.5/0.25/0.19 s. A field of view of 3 x 3 cm<sup>2</sup>, a matrix size of 256 x 128 corresponding to 177 μm x 234 μm in plane resolution and 2 slices centered in the tumor with a thickness of 1.5 mm were used, for an acquisition time of about 17 min.

To evaluate the perfusion in the tumor 24 h after the treatment, a Dynamic contrast Enhanced DCE perfusion protocol was set-up: T<sub>1</sub>-weighted magnetic resonance images were sequentially acquired before (5 images) and after the bolus injection of a common gadolinium based contrast agent (gadoterate meglumine, Dotarem®, Guerbet, France) at a dose of 0.25 mmol/kg. The imaging protocol consisted of a 2D-FLASH T<sub>1</sub> weighted gradient echo sequence with TR/TE = 100/3 msec, a flip angle of 60°, a 128 x 128 matrix, a resolution of 234 x 234 μm<sup>2</sup>/pixel, 4 slices of 2 mm thickness, 70 dynamic scans, giving a temporal resolution of 12.8 s per time point. This sequence was repeated 3 times in a row to obtain a 45 min monitoring.

**MRI data analysis:** The tumor volume was measured from the T<sub>2</sub>\*-weighted images: each slice was opened in the ImageJ software (National Institutes of Health, Bethesda) using the plugin BrukerOpener and the Region Of Interest (ROI) of the tumor was delineated to provide in each slice a surface expressed in mm<sup>2</sup>. Knowing that the thickness of the slice was 1 mm, the tumor volume was obtained by adding the volume calculated for each slice to provide a final volume in mm<sup>3</sup>. The normalized volume of the tumor was then calculated at each time point by dividing the volume of the tumor by one of the tumor at D0.

To compare the efficiency of accumulation of the CA4P-UML depending on the treatment group, the previously described post-processing methodology %I<sub>0.25</sub> was used [11]. Briefly, the pixel intensity distribution of each tumor was obtained from the T<sub>2</sub>-weighted images and the

percentage of pixels under the value  $I_{0.25} = 0.25 \times (\text{Intensity}_{\max} - \text{Intensity}_{\min})$  was calculated and noted % $I_{0.25}$ .

$T_1$  relaxation times were calculated from the  $T_1+T_2$  mapping acquired before the perfusion protocol. The values were computed in the perfusion processing.

The perfusion of the tumor was evaluated by modeling the time course of the contrast agent concentration in the tumor following the bolus injection. We applied the Tofts-Kermode model [28] implemented in Matlab, in which the body is divided into different compartments: intravascular, whole-body extracellular space, tumor extracellular space, and kidneys. For a bolus injection experiment, the concentration of the contrast agent in the plasma  $C_p(t)$ , (in units of mL/L), is represented by a bi-exponential equation. The exchange of the contrast material between the intravascular and extra-cellular space depends upon two parameters:  $v$  – the extracellular volume fraction, accessible to the contrast agent, which is incapable of entering into cells and  $K$  – the transcapillary transfer constant equal to  $PS/V$  (where  $P$  is the microvascular permeability,  $S$  is the microvascular surface area and  $V$  is the pixel volume).

The Mann-Whitney non-parametric test was used to compare two by two groups with a low number of samples [29].

## 10. Histology

Three mice from each group (control and treated) were sacrificed 24 h after treatment, the tumor was removed and quickly frozen in isopentane cooled with liquid nitrogen. Ten-micron frozen tissue sections were obtained in the central axial plan of the tumor, placed on Polysine slides (Polysine®, CML, Nemours, France) and kept frozen before staining. In each slice section, ten representative images were undertaken and analyzed. CD31 with haematoxylin counterstain protocol was performed and image digitization was made under identical lighting conditions using a microscope to ensure that analyses from different conditions were comparable.

**Microvascular density (MVD):** The quantification of the vascularization was performed using the anti-CD31 (PECAM1) labelling consisting of a three-step procedure as previously described[30]. The quantification of the number of vessels per square millimeter ( $\text{mm}^2$ ) was computed with a specific macro under ImageJ software [31] as previously described [25].

**Cellularity:** The quantification of the number of cells was analyzed on the same picture using a specific macro developed by ImageJ. Briefly, the contrast was enhanced (saturated=50, equalize), the background was subtracted (rolling=100 lights), the image was despeckled and transformed in 8-bit. Then, the brightness were settled from 69 to 255 and the image was binarized. Finally, a watershed filter was applied to a separate nucleus and the particles with a size ranging from 20 to 1000 and a circularity from 0 to 1 were measured [25].

**Statistical analysis:** Histological result was expressed in mean  $\pm$  SEM, One-way analysis of variance and Bonferroni's Multiple Comparison Test was applied to determine the significance of the result, P-value Summary : < 0.001 Extremely significant \*\*\*; 0.001 to 0.01 Very significant \*\*; 0.01 to 0.05 Significant \*; >0.05 Not significant ns.

## Results and Discussion

Figure 1 illustrates the rationale of the approach: magnetic liposomes that could be targeted to the tumor by using a magnet, stimulated by HIFU to trigger the CA4P release by local hyperthermia and MRI monitoring of the treatment efficiency.

## 1. Preparation of CA4P-UML and in vitro drug release

We previously adapted a reverse-phase evaporation method to obtain ultramagnetic liposomes (UML) with a high ratio of iron per lipids content, which are essential for obtaining the local accumulation of the UML in the tumor [12,32]. The vascular disrupting agent, CA4P, which is a water-soluble drug, was selected to be encapsulated in the aqueous part of the liposome together with the magnetic nanoparticles (MNP). Since the MNP are stabilized by citrate molecules, there was no interaction between the negatively charged CA4P and the MNP. The lack of interaction between CA4P and MNP was verified by titration of the drug released after ultrafiltration of a suspension of MNP and CA4P.

The amount of CA4P in CA4P-UML was adjusted in order to obtain the highest encapsulation of CA4P while the encapsulation of MNP remain the same than for UML.

The Transmission Electron Microscopy (TEM) observations confirmed the liposome structure with the presence of spherical and dense aggregates of MNP for both UML and CA4P-UML (Figure 2-A and B). The presence of the bilayer around these magnetic aggregates was already established in previous studies by cryo-TEM [11,12]. One can note a little modification of the morphology of the UML after encapsulation of CA4P (Figure 2B), however, drying artefacts related to the sample preparation can occur. The Tunable Resistive Pulse Sensing (TRPS) measurement of the liposome size correlates these observations with a diameter of  $230 \pm 46$  nm and  $209 \pm 56$  nm for UML and CA4P-UML respectively without significant difference (Figure 2C). Polydispersity was also comparable between both preparations. At the end of the preparation, magnetic sorting was systematically used to collect magnetic liposomes. This step allows the separation between the magnetic liposomes and the supernatant containing both free CA4P and free magnetic nanoparticles which are not attracted at the same kinetic that UML. Iron concentration was measured by atomic absorption spectroscopy. Thereafter, an ultrafiltration step is required for the recovering of CA4P, the amount of drug successfully encapsulated inside UML was determined. The mean encapsulation of MNP and CA4P was calculated from 10 synthesis and was found to be 3.3 mM of CA4P for 1.5 M of iron. The relaxivities of both free MNP and UML were measured at 7T in a previous work [11] showing an expected much higher  $r_2$  values by a factor of 2.9 for UML.

The encapsulation of CA4P in magnetic liposomes was not reported before and we found that CA4P was encapsulated in UML with a ratio CA4P/lipid of 0.18 and a ratio iron/lipid of 83. These ratios are consistent with independent CA4P/lipid and the iron/lipid ratio reported in the literature. Few examples of liposomes encapsulating CA4P have been reported in the literature. By comparison, Pattillo *et al.* encapsulated CA4P in liposomes with a CA4P/lipids molar ratio of 0.32 [10]. Other authors encapsulated the hydrophobic CA4 in liposome membranes and obtained CA4/lipid molar ratio of 0.16 for Nallamotheu *et al.* [33] and 0.40 for Zhang *et al.* [34]. Jiang *et al.* had encapsulated 5% of CA4P in their liposomes [35], Venegas has synthesized the same formulations as Pattillo's [36]. and Daswani *et al.* have obtained 0.25-0.5mM of CA4P in archaeal tetraether liposomes (archaeosomes) [37].

The encapsulation of CA4P in CA4P-UML was thus found to be lower than in some literature, but CA4P-UML contained a high volume ratio of MNP. As regard to the Patillo's reference, in our last study published in 2019, the amount of CA4P injected to obtain in vivo antitumor efficacy was 25mg/kg while we could reduce in our present work this amount to 0.65 mg/kg while keeping an antitumoral effect.

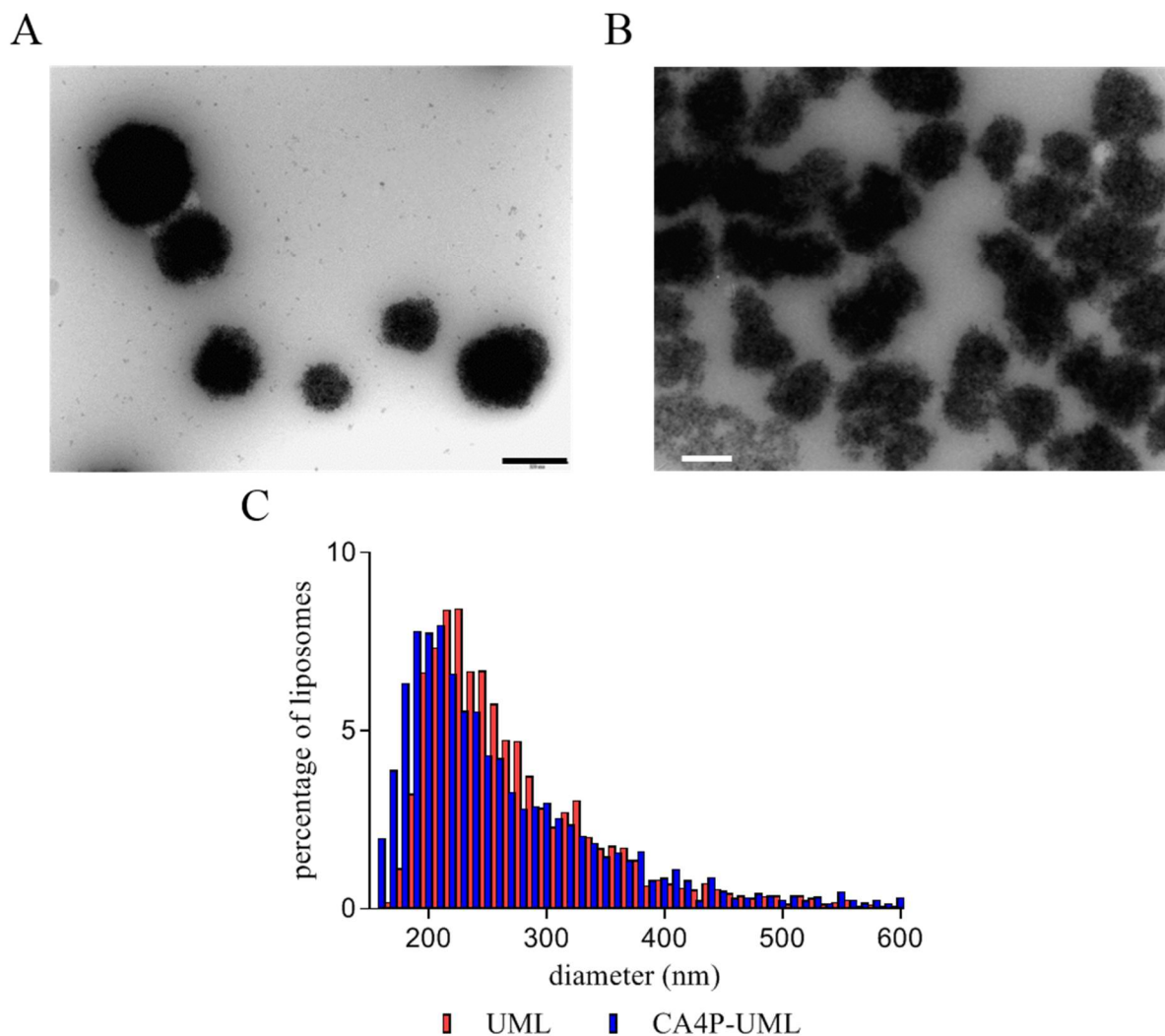


**Figure 2.** TEM images of UML (A) and CA4P-UML (B) and their size distributions measured by TRPS (C). Bars on (A) and (B) images indicate a scale of 200 nm.

The CA4P release from the liposomes was investigated at physiological temperature by titration of the CA4P concentration in the supernatant after liposome ultrafiltration. A passive release of the CA4P from CA4P-UML was observed which corresponds to  $3.5 \pm 0.1\%$  after 30 min, which increased to  $6.2 \pm 0.05\%$  and  $9.4 \pm 0.2\%$  after 45 min and 60 min respectively (Figure 3).

The HIFU-triggered release is a recent strategy to increase drug delivery from nanomedicine [38]. CA4P-UML are thermosensitive liposomes with a transition temperature of the bilayer at  $43^\circ\text{C}$  [12]. The thermal behavior of DPPC/DSPC/DSPE-PEG bilayer was already investigated by DSC and published [39]. For this lipid composition without MNP a transition temperature of  $43^\circ\text{C}$  was measured. Therefore, to enhance the CA4P release, the previously developed HIFU sequences (Table 1) were used to increase the temperature of the solution from  $37^\circ\text{C}$  to  $43^\circ\text{C}$  for 5 min. To mimic the *in vivo* conditions, CA4P-UML were placed in a water bath at  $37^\circ\text{C}$  for 30 min (duration of the magnetic targeting in *in vivo* experiments rationalized by the blood circulation of the ULMs post injection during less than one hour [11]) before shooting the HIFU sequences. We measured a HIFU triggered CA4P release of  $12.8 \pm 0.2\%$  and  $17.0 \pm 0.1\%$  at 15 and 30 min post-HIFU (45 and 60 min respectively after insert of CA4P-UML in the water bath at  $37^\circ\text{C}$ ). From Figure 3, it can be seen that the release of HIFU was doubled 15 min after the increase of temperature (i.e from  $6.2\%$  to  $12.8\%$ ). Noteworthy, the release kept

increasing 30 min after HIFU indicates that liposomes remained leaky for that period despite the absence of HIFU and there was a return of temperature to 37°C. This might be explained by the formation of more leaky liposomes once they have been exposed to temperatures close to their transition temperature. In this time range, we do not observe a complete release of the CA4P. In fact, unlike lysolipid-containing liposomes such as ThermoDox® [40], which releases 80% of its content in about 20 seconds at 42°C thanks to the formation of pores, UMLs remain more stable and the increase of permeability observed at the transition temperature is due to the presence of defects between gel and liquid crystal phase domains in the UML membrane. In addition, it has been shown by Daswani *et al.* that the CA4P molecules could associate with each other by  $\pi$  interactions within the liposomes thus limiting their release [37]. This slower release could be advantageous for our treatment strategy providing a sustained release of the drug, eventually avoiding repeated administrations.

Nevertheless, HIFU makes it possible to strongly increase the release of CA4P from CA4P-UML. Furthermore, since ultrasound is focused, it would be possible, *in vivo*, to locate this release only in the targeted biological region.

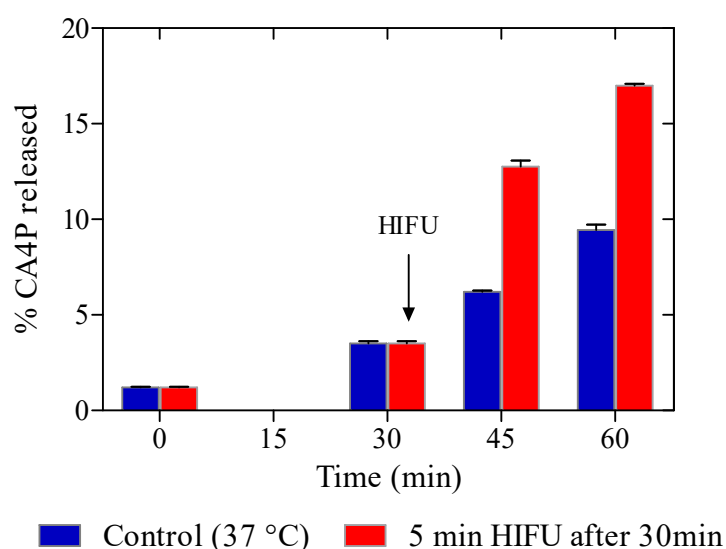


**Figure 3.** CA4P release kinetic of CA4P-UML for control at 37 °C (red) and with 5 min HIFU after 30 min at 37°C (blue)

## 2. *In vitro* evaluation

As explained previously, CA4 prevents the tubulin polymerization into microtubules. Endothelial cells have a characteristic elongated shape but in the presence of CA4, the cytoskeleton of the cell is damaged and the cell morphology evolves to a rounder shape [2]. Therefore, the cell morphology was studied *in vitro* on endothelial cells to evaluate the efficiency of CA4P-UML by measuring the circularity of the cells [41].

By optical microscopy (Figure 4A-D), the blebbing of EA.hy926 endothelial cells was observed 2.5 and 5 h after incubation with CA4P-UML (10  $\mu$ M of CA4P, Figure 4D) as compared to the control (Figure 4A). In opposite, incubation of the cells with UML did not show any effect on the cell shape (Figure 4B). To confirm these microscopic observations, the circularity of each cell was measured and the results were submitted to the Student's t-test to statistically compare the various conditions (Figure 4E). Interestingly, the quantification of the circularity showed a stronger effect of the CA4P when encapsulated inside UML as compared to free CA4P or the

UML has taken as controls. The cytotoxicity of free CA4P, UML and CA4P-UML was also compared for colon tumor cells and hepatic cells in Supporting Information (S2).

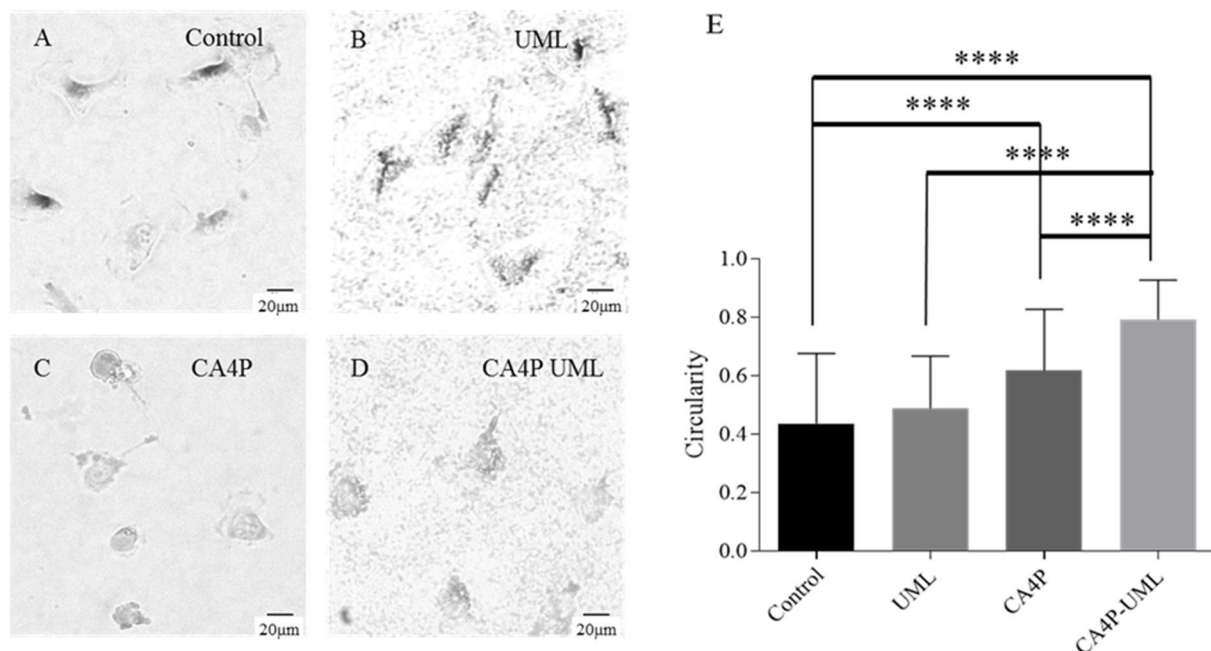


**Figure 4.** Representative pictures of EA.hy926 endothelial cells obtained by optical microscopy after 2.5 h incubation in (A) injection buffer (Control), (B) UML at 5 mM iron, (C) CA4P at 10  $\mu$ M and (D) CA4P-UML at 5 mM of iron and 10  $\mu$ M of CA4P (E) Circularity of the cells after a 2.5 h incubation with injection buffer (Control), UML, CA4P or CA4P-UML. (Mean  $\pm$  SEM) n= 2. Student statistic test: \*\*\*\*: p < 0.0001.

### 3. *In vivo* tumor targeting

The *in vivo* tumor targeting was assessed by using a post-processing methodology previously described [11]. On  $T_2^*$ - weighted images, the pixel intensity distribution was measured in order to calculate the  $\%I_{0.25}$  which was taken as the parameter of reference to compare the different groups (Figure 5). Briefly, the pixel intensity distribution of each tumor was obtained from the  $T_2$ -weighted images and the percentage of pixels under the value  $I_{0.25} = 0.25 \times (\text{Intensity}_{\text{max}} - \text{Intensity}_{\text{min}})$  was calculated and noted  $\%I_{0.25}$ . The  $\%I_{0.25}$  in the tumor was similar for control and the tumors treated with HIFU (2.2 % and 2.4 % respectively). As soon as CA4P-UML were injected, the  $\%I_{0.25}$  increased reflecting the passive accumulation of the magnetic liposomes into the tumor. This result is not surprising as the CT26 cell line was selected [23] for its high neoangiogenic component that ensures distribution of liposomes into the tumor, thanks to the enhanced permeability and retention effect [42]. HIFU reduces non significantly the signal within the tumor area; our hypothesis, here, is that the HIFU induced a release of the CA4P and perhaps a recirculation of the CA4P-UML. Nevertheless, the release of CA4P occurred while/before this recirculation and provide an increase of therapeutic effect. The addition of a magnetic targeting (MT) on one side of the animal improved the accumulation of UML into the tumor, independently of the HIFU application, with a  $\%I_{0.25}$  increasing from 25.5% for passive accumulation to 41.8% with MT, a factor of 1.6. The efficiency of MT is consistent with our previous results [11].

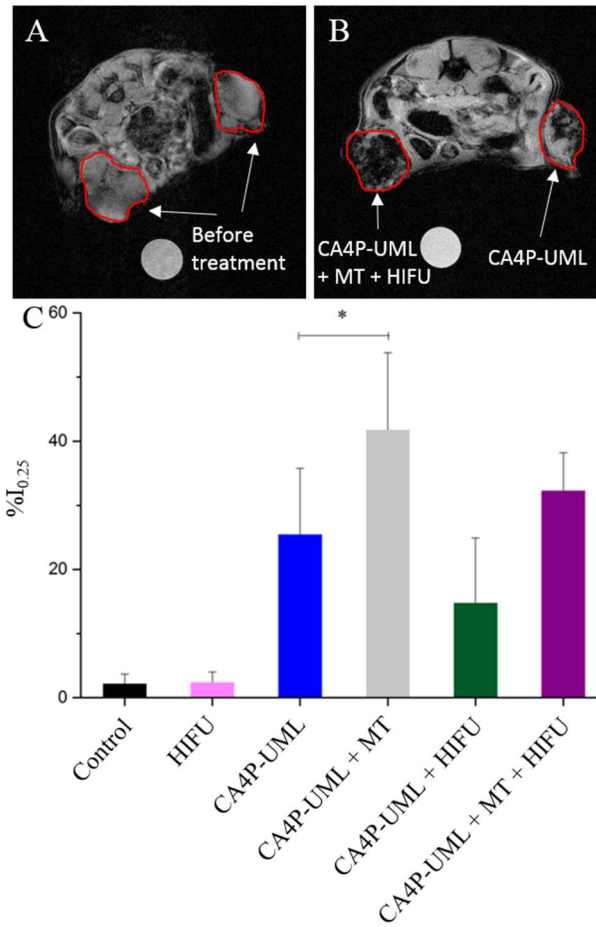


**Figure 5.**  $T_2^*$ -weighted MRI images of tumors before (A) and after (B) the treatment. CA4P-UML + MT + HIFU on the left tumor and CA4P-UML on the right tumor. (C) Comparison of  $\%I_{0.25}$  values (mean + SD) for the different groups the day of the treatment. Mann-Whitney statistic test: \*:  $p < 0.05$ .

#### 4. *In vivo* tumor efficacy

The tumor volume was measured from MRI images acquired by a  $T_2^*$ -weighted FLASH sequence and synchronized with the respiratory cycle of the mouse. Examples of  $T_2$ -weighted MRI images illustrating the tumor volume depending on treatment is available in Supporting Information (Figure S5). These acquisitions were recorded the day of treatment D0 and then 1, 4 and 7 days later. The volume of each tumor was normalized by its volume at D0 (Figure 6A and 6B). The values of normalized tumor volume depending on treatment at 1, 4 and 7 days after treatment are given in supporting information (Table S6).

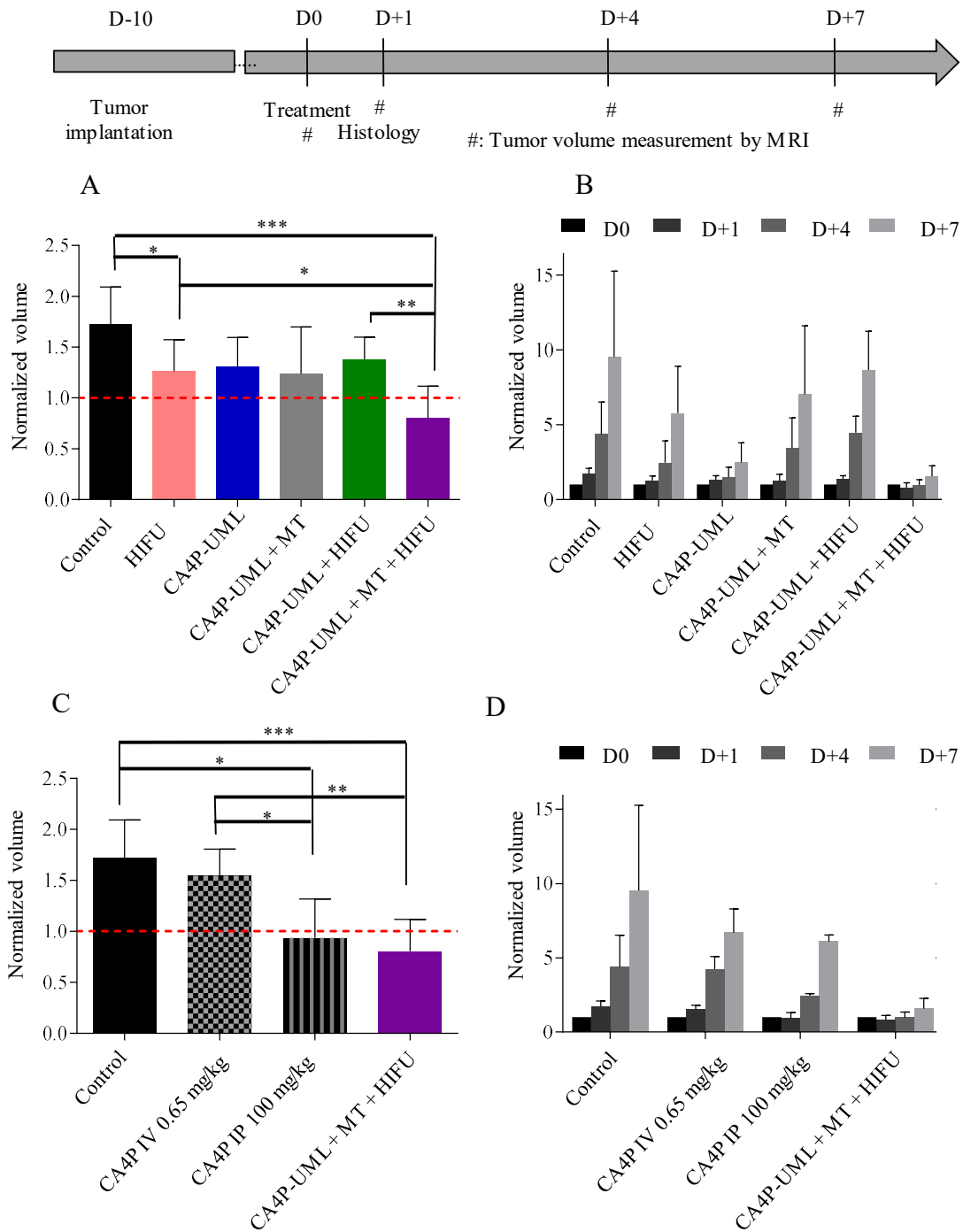


**Figure 6.** MRI measurement of tumor volume with (A) and (C) normalized tumor volume 24 h after treatment, (B) and (D) tumor volume evolution at day 0 (D0), 24 h after treatment (D+1), 4 days after treatment (D+4) and 1 week after treatment (D+7). Mann-Whitney statistic test: \*:  $p < 0.05$ , \*\*:  $p < 0.01$  and \*\*\*:  $p < 0.001$ .

Twenty-four-hour after treatment, HIFU alone had a small growth inhibition effect (normalized volume of  $1.3 \pm 0.3$ ,  $n = 8$ ) as compared with the control tumors ( $1.7 \pm 0.4$ ,  $n = 8$ ). A limited effect was found with the following treatment: CA4P-UML treatments ( $1.3 \pm 0.3$ ,  $n = 6$ ), CA4P-UML + MT ( $1.2 \pm 0.4$ ,  $n = 7$ ) and CA4P-UML + HIFU ( $1.4 \pm 0.2$ ,  $n = 7$ ) although the differences with the controls are not significant. Noteworthy, only the complete therapeutic

protocol CA4P-UML + MT + HIFU showed a significant growth inhibition effect ( $0.8 \pm 0.3$ ,  $n = 6$ ) at 24 h (Figure 6A).

In the literature, CA4P is injected intraperitoneally at 100 mg/kg [43,44], i.e. a dose 150 times greater than the one used in this study, which is 0.65mg/kg. Therefore, the efficacy of CA4P-UML + MT + HIFU treatment was compared with the intraperitoneal injection of free CA4P at 100 mg/kg. In addition, in order to evaluate the contribution of the CA4P-UML, therapeutic strategy with magnetic targeting and HIFU release, the equivalent quantity of CA4P (0.65 mg/kg) was injected by the systemic route as done for CA4P-UML. The effect on tumor responses of these two free CA4P injections was compared to the complete protocol (Figure 6C). Intravenous CA4P injection at 0.65 mg/kg ( $n = 4$ ) had no effect on tumor growth as regard to the untreated control at D+1. CA4P administered intraperitoneally at 100 mg/kg ( $n = 3$ ) had an efficacy similar to CA4P-UML + MT + HIFU injected at a dose 150 times lower (0.65 mg/kg). These data showed that the combination strategy proposed allows obtaining a better therapeutic outcome on the tumor volume regression while reducing the dose of CA4P 150 fold. This is obviously of high interest to reduce toxicity issues related to the drug.

A longitudinal follow-up has been performed over one week, although no significant differences could be evidenced 4 and 7 days after the protocol (Figure 6B, D). The absence of significant differences after 4 days is not surprising as CA4P is a vascular disrupting agent. Devascularisation can affect the vascular network and reduce the tumor growth after 24 h as we have already observed in our studies [24]. However, to obtain a longer term effect, the administration should be repeated, as it is also the case for most cytotoxic. The tumor has several means to oppose the effect of the treatment. The effect of antivascular disrupting agent alone is usually not sufficient and require the combination with other anticancer agents, the vessels in periphery are indeed more resistant to this therapy as they are more mature [45]. Nevertheless, in clinic, the patients would be treated previously with infusion of cytostatics before our protocol would be proposed. A significant effect at days 4 and 7 was therefore not expected after one single protocol of treatment. In opposite, the demonstration of a significant effect at 24 h of the complete protocol that we have conceived in this study meaning CA4P-UML + MT + HIFU is a relevant proof of concept from which we did not expect to be able to lower that much the amount of CA4P used, which is 150 times less than the usual administration [43,44]. This looks extremely promising, and shows that increasing the various beneficial effects of magnetic targeting, concentration of the drug in the tumor area and triggering the release could be a promising approach.

## 5. Assessment of the antivascular effect of CA4P

In order to better understand the impact of the therapy on the tumor, *in vivo* tumor function studies were carried out with the evaluation of tumor perfusion by MRI, 24 h after treatment (Figure 7). For this purpose, Dotarem®, a commercial MRI contrast agent, was injected intravenously during a Dynamic Contrast Enhancement (DCE) experiment [28]. The presence of Dotarem® in a tissue shortens its  $T_1$  relaxation time and causes a hyper-signaling dedicated  $T_1$ -weighted MRI sequence (DCE), which is monitored to observe the kinetics of extravasation and perfusion of this agent in the tumor. At 11 days after their implantation, the untreated CT26 tumors show a chaotic vascularization. Dotarem®, therefore, perfuses efficiently and rapidly accesses the tumor causing a rapid signal increase. The contrast agent then undergoes a slower clearance, causing a drop of signal in the tumor. On the contrary, after an anti-vascular treatment, tumor blood vessels have been shut down since the antivascular agent principally acts on tumor vessels as regard to normal vascularization [46], Dotarem® is therefore expected to exhibit a lower accumulation in the tumor. Examples MRI signal evolution in the tumor after injection of Dotarem® for a control CT26 tumor and a CT26 tumor after full treatment are given in supporting information (Figure S7). A mathematic bi-compartmental model developed by

Tofts and Kermode [28] allows computing quantitative microperfusion values to characterize the perfusion impacted by an antivascular therapy.

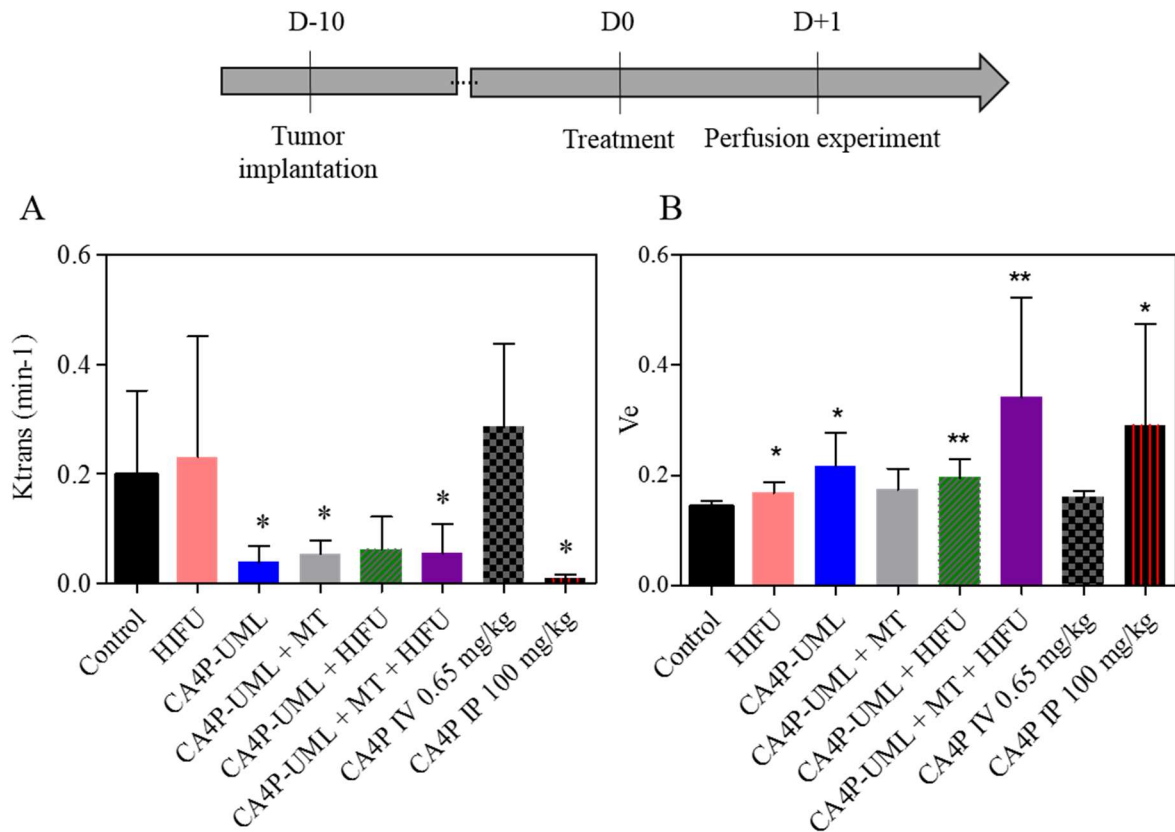


**Figure 7.** (A) Transcapillary transfer constant ( $K_{trans}$ ) and (B) extracellular volume fraction ( $V_e$ ) of CT26 tumors 24 h after treatment computed from perfusion in vivo MRI acquisition and processing methods. Mann-Whitney statistic test comparison with the control: \*:  $p < 0.05$  and \*\*:  $p < 0.01$ .

The  $K_{trans}$  parameter represents the transfer rate of blood contrast agent (here Dotarem®) from the blood to the interstitial space according to the Tofts-Kermode model. Thus, it depends on the permeability of the capillaries but also on the blood flow. DCE infusion studies using a relatively small contrast agent such as Dotarem® have been shown to reflect the difference in blood flow due to the high permeability of the capillaries to this small contrast agent [47]. In this study, a significant decrease in the permeability constant  $K_{trans}$  was observed 24 h after the injection of CA4P-UML. No significant contribution of magnetic targeting and HIFU was found in this parameter (Figure 7A). CA4P is a vascular destruction agent (VDA) and causes blood vessel blockage and decreases blood flow [2]. Thus, the decrease of  $K_{trans}$  24 h after the injection of CA4P-UML shows the effectiveness of treatment on the blockage of tumor blood vessels. Treatment with free CA4P at 0.65 mg/kg had no effect on  $K_{trans}$ , unlike the dose of 100 mg/kg, which caused a fall in  $K_{trans}$  comparable to that observed with CA4P-UML. These data comfort the fact that CA4P should be encapsulated and released locally to exert an effect at the low dose of 0.65 mg/kg.

Besides, the extracellular volume fraction was significantly increased only for the complete protocol CA4P-UML + MT + HIFU and the injection of free CA4P at 100 mg / kg (Figure 7B). The increase in the extracellular volume fraction may be explained by a decrease in cellularity or the appearance of hemorrhagic necrosis.

## 6. Histology Results

In order to confirm these MRI observations, histological analyses of the tumors were performed for the main experimental condition 24 h after treatment. Histological staining of the vascularization (CD31) and the cellular density was undertaken. Figure 8 presents the method used for the segmentation of these histological pictures (Figure 8A) and the result obtained in term of microvascular density (Figure 8B, MVD, number of vessels /mm<sup>2</sup>) and cellularity (Figure 8C, cells/mm<sup>2</sup>). In Figure 8B, the significant decrease of the MVD for the complete treatment was consistent with the significant diminution of Ktrans. In a second time (Figure 8C), an evaluation of the number of cells per mm<sup>2</sup> was made on the same picture. A diminution of the number of cells was observed for all the conditions which are in concordance with the increase of the extracellular volume (Ve) measured by MRI.

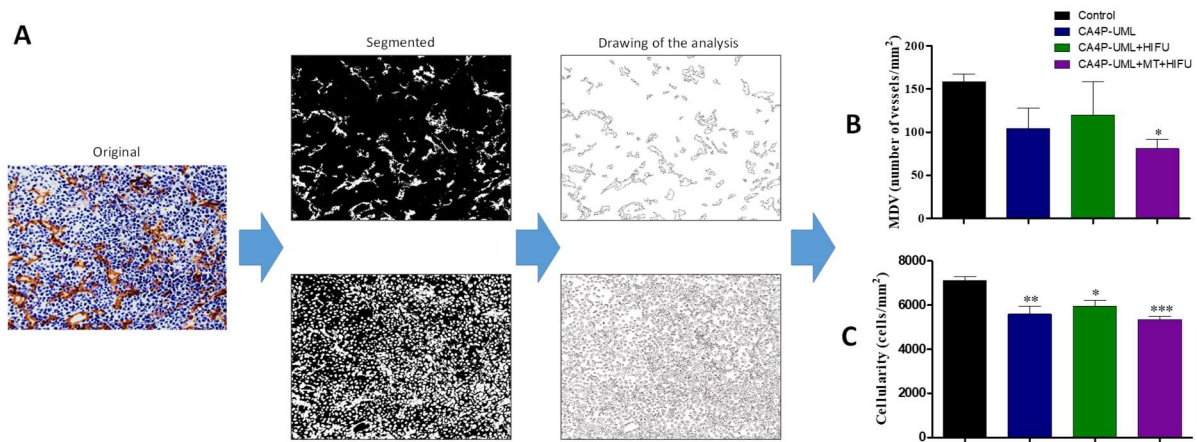


**Figure 8.** Histology results, (A) Method of segmentation realized and used to quantify the vessel density (up) and the cellularity (down). Microvascular density (B) and cellularity (C) quantification for the control (black), CA4P-UML (blue), CA4P-UML + HIFU (green) and CA4P-UML+MT+HIFU (violet) groups 1 day after treatment. Mean  $\pm$  SEM, 1 way anova with Dunnett's Multiple Comparison Test, \*,  $P \leq 0.05$ ; \*\*,  $P \leq 0.01$ ; \*\*\*,  $P \leq 0.001$ .

CA4P is an antivascular agent. It is known to induce necrosis at the center of the tumor and fibrosis in the periphery of the tumor [43]. This was evidenced earlier on CT26 tumors by our group [24]. In this type of study, obtention of significant results is impaired by the fact that the effect of CA4P leaves a mixture of viable cells and necrotic cells, which is different from the effect of cytotoxics. Searching for the impact of CA4P on the stiffness and elasticity of the tumor, we had to select reduced areas of interest to find discrepancies [30]. In this study, the quantification of the parameters Ktrans and Ve by MRI in the overall tumors nevertheless led to significant results as soon as CA4P was present in the tumor at a sufficient level. Indeed, CA4P injected intravenously was not sufficient to impact these parameters. Moreover, the effect on tumor growth inhibition was even more convincing with the need for a large amount of antivascular agent to obtain an effect. A similar therapeutic effect was obtained here with the combination strategy at a dose reduced 150 folds. This looks extremely promising, and may result from a combination of mechanisms: the accumulation of a higher amount of liposomes, thanks to the magnetic targeting, a particularly stable formulation with the presence of potential  $\pi$  interactions between CA4P molecules leading to a sustained release of CA4P from the liposomes, maintaining the drug in the tumor environment for a longer period of time. The HIFU was used to release CA4P from the liposomes, but it is also known that mild hyperthermia is a strategy to increase blood vessel pressure and can, therefore, influence the tumor

microenvironment [48], potentially enhancing the effect of the combination therapy. In order to combine drug delivery and ultrasounds, parameters must be calibrated according to the specific environment to avoid damaging healthy tissues [38].

In the literature, HIFU was already described to trigger drug release [49–51] and magnetic targeting was also evidenced [12]. In most cases, however, magnetic particles are used to provide a means to monitor HIFU by MRI [52]. Magnetic targeting associated with HIFU delivery of 5-Fluorouracil from nanocapsules has been used previously to improve the therapy compared to the chemotherapy alone [53]. The effect of the cytotoxic agent was enhanced, thanks to the combined therapy.

The combination proposed here is to our knowledge the first example of magnetic targeting associated with HIFU triggered delivery of an antivascular agent in order to starve the tumor, with *in vivo* MRI image-guided therapy. We show here the potential of the strategy which could obviously be improved. Several parts could benefit from improvement, designing magnets with a magnetic gradient better delineated to the tumor to improve the targeting effect, applying mobile HIFU to increase the temperature in different areas where nanoparticles have accumulated in the tumor, or to repeat the HIFU shots as we have observed by MRI that UML remain several days within the tumor. Finally, as HIFU has been shown in some studies to induce an immunological effect [54], this would be extremely interesting in the next future to work on a protocol with repeated administrations during the first week to induce this combinative effect which could there induce a real benefit and avoid recurrence. This, obviously, is a whole complete study to understand the mechanism of the anti-tumor response involved.

## Conclusions

We propose here a new combination therapy for tumor treatment using thermosensitive liposomes encapsulating iron oxide nanoparticles with a dual effect of magnetic targeting and MRI monitoring. These liposomes co-encapsulate an antivascular disrupting agent in order to starve the tumor and modify its microenvironment. The temperature transition of the lipids composing the liposomes was chosen around 43°C, which can be achieved by HIFU providing focalized mild hyperthermia. Only the full combination of magnetic liposome containing CA4P + magnetic targeting + local ultrasound release provided a significant decrease of the tumor volume. This was shown 24 h post-therapy after one single treatment, using 150 fold less antivascular disrupting agent than the usual administration. This proof of concept is highly interesting as it shows that ultramagnetic liposomes containing CA4P with or without magnetic targeting, or HIFU alone are not as efficient in inhibiting tumor growth, meaning that each component of this combination therapy had a crucial role to play. MRI bioimaging evidenced the efficiency of this therapy *in vivo* with the functional alteration of the vasculature, by decreased permeability as well as the reduction of tumor growth. This was also demonstrated by the fact that tumor growth inhibition was in adequation with what was expected from CA4P delivery, meaning an alteration of the vascular permeability, reduction of the vascularization, a diminution of the functional cells and an extracellular volume increase.

## Acknowledgements

*In vivo* imaging was performed at the LIOPA UTCBS bioimaging facility from Life Imaging Facility of Paris Descartes University (Plateformes Imageries du Vivant – PIV). The GDR AIM is also acknowledged as well as the CNRS, Inserm and ENSCP ChimieParistech.

## Funding

This work was supported by the LabEx MiChem part of French state funds managed by the ANR within Le Programme Investissements d’Avenir under reference ANR-11-IDEX-0004-02. The program IDEX Imageries du Vivant of Sorbonne Paris Cité, the CNRS, Inserm are also acknowledged as well as the Institut Pasteur Weizmann for financial support. France Life Imaging provided financial support for the MRI guided focused ultrasound and *in vivo* thermometry experiments presented as supplementary data.

## References

- [1] G.R. Pettit, S.B. Singh, E. Hamel, C.M. Lin, D.S. Alberts, D. Garcia-Kendal, Isolation and structure of the strong cell growth and tubulin inhibitor combretastatin A-4, *Experientia*. 45 (1989) 209–211. <https://doi.org/10.1007/BF01954881>.
- [2] G.M. Tozer, C. Kanthou, B.C. Baguley, Disrupting tumour blood vessels, *Nat. Rev. Cancer*. 5 (2005) 423–435. <https://doi.org/10.1038/nrc1628>.
- [3] D.W. Siemann, D.J. Chaplin, M.R. Horsman, Vascular-targeting therapies for treatment of malignant disease, *Cancer*. 100 (2004) 2491–2499. <https://doi.org/10.1002/cncr.20299>.
- [4] E.B. Garon, F.F. Kabbinavar, J.A. Neidhart, J.D. Neidhart, N.Y. Gabrail, M.R. Oliveira, S.P. Lu, J. Balkissoon, D. Geffen, Randomized phase II trial of a tumor vascular disrupting agent fosbretabulin tromethamine (CA4P) with carboplatin (C), paclitaxel (P), and bevacizumab (B) in stage IIIb IV, in: ASCO Annu. Meet. J Clin Onc, 2010: p. 7587.
- [5] B.J. Monk, M.W. Sill, J.L. Walker, C.J. Darus, G. Sutton, K.S. Tewari, L.P. Martin, J.M. Schilder, R.L. Coleman, J. Balkissoon, C. Aghajanian, Randomized Phase II Evaluation of Bevacizumab Versus Bevacizumab Plus Fosbretabulin in Recurrent Ovarian, Tubal, or Peritoneal Carcinoma: An NRG Oncology/Gynecologic Oncology Group Study, *J. Clin. Oncol.* 34 (2016) 2279–2286. <https://doi.org/10.1200/JCO.2015.65.8153>.
- [6] R. Granata, L.D. Locati, L. Licitra, Fosbretabulin for the treatment of anaplastic thyroid cancer, *Future Oncol.* 10 (2014) 2015–2021. <https://doi.org/10.2217/fon.14.154>.
- [7] R. Grisham, B. Ky, K.S. Tewari, D.J. Chaplin, J. Walker, Clinical trial experience with CA4P anticancer therapy: focus on efficacy, cardiovascular adverse events, and hypertension management, *Gynecol. Oncol. Res. Pract.* 5 (2018) 1. <https://doi.org/10.1186/s40661-017-0058-5>.
- [8] W.J. Yang, P. Zhou, L. Liang, Y. Cao, J. Qiao, X. Li, Z. Teng, L. Wang, Nanogel-Incorporated Injectable Hydrogel for Synergistic Therapy Based on Sequential Local Delivery of Combretastatin-A4 Phosphate (CA4P) and Doxorubicin (DOX), *ACS Appl. Mater. Interfaces*. 10 (2018) 18560–18573. <https://doi.org/10.1021/acsami.8b04394>.

- [9] Q. Liping, Wu; Liyan, Reverse micelles-in-microspheres with sustained release of water-soluble combretastatin A4 phosphate for S180 tumor treatment, *J. Mater. Chem. B.* 4 (2016). <https://doi.org/10.1039/x0xx00000x>.
- [10] C.B. Pattillo, B. Venegas, F.J. Donelson, L. Del Valle, L.C. Knight, P.L.G. Chong, M.F. Kiani, Radiation-guided targeting of combretastatin encapsulated immunoliposomes to mammary tumors, *Pharm. Res.* 26 (2009) 1093–1100. <https://doi.org/10.1007/s11095-009-9826-1>.
- [11] C.J. Thébault, G. Ramniceanu, A. Michel, C. Beauvineau, C. Girard, J. Seguin, N. Mignet, C. Ménager, B.-T. Doan, In Vivo Evaluation of Magnetic Targeting in Mice Colon Tumors with Ultra-Magnetic Liposomes Monitored by MRI, *Mol. Imaging Biol.* (2018). <https://doi.org/10.1007/s11307-018-1238-3>.
- [12] G. Béalle, R. Di Corato, J. Kolosnjaj-Tabi, V. Dupuis, O. Clément, F. Gazeau, C. Wilhelm, C. Ménager, Ultra magnetic liposomes for MR imaging, targeting, and hyperthermia, *Langmuir.* 28 (2012) 11834–11842. <https://doi.org/10.1021/la3024716>.
- [13] A.M. Derfus, G. von Maltzahn, T.J. Harris, T. Duza, K.S. Vecchio, E. Ruoslahti, S.N. Bhatia, Remotely Triggered Release from Magnetic Nanoparticles, *Adv. Mater.* 19 (2007) 3932–3936. <https://doi.org/10.1002/adma.200700091>.
- [14] K. Cai, Z. Luo, Y. Hu, X. Chen, Y. Liao, L. Yang, L. Deng, Magnetically Triggered Reversible Controlled Drug Delivery from Microfabricated Polymeric Multireservoir Devices, *Adv. Mater.* 21 (2009) 4045–4049. <https://doi.org/10.1002/adma.200900593>.
- [15] M. Liu, Z. Wang, S. Zong, H. Chen, D. Zhu, Y. Zhong, Y. Cui, Remote-controlled DNA release from Fe<sub>3</sub>O<sub>4</sub>@Au nanoparticles using an alternating electromagnetic field, *J Biomed Nanotechnol.* 11 (2015) 979–987. <https://doi.org/doi:10.1166/jbn.2015.2013>.
- [16] R. Massart, Preparation of aqueous magnetic liquids in alkaline and acidic media, *IEEE Trans. Magn.* 17 (1981) 1247–1248. <https://doi.org/10.1109/TMAG.1981.1061188>.
- [17] N. Fauconnier, A. Bee, J. Roger, J.N. Pons, Synthesis of aqueous magnetic liquids by surface complexation of maghemite nanoparticles, *J. Mol. Liq.* 83 (1999) 233–242.
- [18] S. Lefebure, E. Dubois, V. Cabuil, S. Neveu, R. Massart, Monodisperse magnetic nanoparticles: Preparation and dispersion in water and oils, *J. Mater. Res.* 13 (1998) 2975–2981. <https://doi.org/10.1557/JMR.1998.0407>.
- [19] C.-J.S. Edgell, C.C. McDonald, J.B. Graham, Permanent cell line expressing, *Proc. Natl. Acad. Sci. U. S. A.* 80 (1983) 3734–3737. <https://doi.org/10.1073/pnas.80.12.3734>.
- [20] C.A. Schneider, W.S. Rasband, K.W. Eliceiri, NIH Image to ImageJ: 25 years of image analysis, *Nat. Methods.* 9 (2012) 671–675. <https://doi.org/10.1038/nmeth.2089>.
- [21] Student, The Probable Error of a Mean, *Biometrika.* 6 (1908) 1. <https://doi.org/10.2307/2331554>.
- [22] J. Seguin, B.-T. Doan, H. Latorre Ossa, L. Jugé, J.-L. Gennisson, M. Tanter, D. Scherman, G.G. Chabot, N. Mignet, Evaluation of Nonradiative Clinical Imaging Techniques for the Longitudinal Assessment of Tumour Growth in Murine CT26 Colon Carcinoma., *Int. J. Mol. Imaging.* 2013 (2013) 983534. <https://doi.org/10.1155/2013/983534>.
- [23] J. Seguin, C. Nicolazzi, N. Mignet, D. Scherman, G.G. Chabot, Vascular density and endothelial cell expression of integrin alpha v beta 3 and E-selectin in murine tumours, *Tumour Biol.* 33 (2012) 1709–1717.
- [24] L. Jugé, B.-T. Doan, J. Seguin, M. Albuquerque, B. Larrat, N. Mignet, G.G. Chabot, D. Scherman, V. Paradis, V. Vilgrain, others, Colon tumor growth and antivascular treatment in mice: complementary assessment with MR elastography and diffusion-weighted MR imaging, *Radiology.* 264 (2012) 436–444.
- [25] J. Seguin, N. Mignet, H. Latorre Ossa, M. Tanter, J.-L. Gennisson, Evaluation of Antivascular Combretastatin A4 P Efficacy Using Supersonic Shear Imaging Technique

- of Ectopic Colon Carcinoma CT26, *Ultrasound Med. Biol.* 43 (2017) 2352–2361. <https://doi.org/10.1016/j.ultrasmedbio.2017.05.013>.
- [26] B. Larrat, M. Pernot, J.F. Aubry, E. Dervishi, R. Sinkus, D. Seilhean, Y. Marie, A.L. Boch, M. Fink, M. Tanter, MR-guided transcranial brain HIFU in small animal models, *Phys. Med. Biol.* 55 (2010) 365–388. <https://doi.org/10.1088/0031-9155/55/2/003>.
- [27] R. Magnin, F. Rabusseau, F. Salabartan, S. Mériaux, J.F. Aubry, D. Le Bihan, E. Dumont, B. Larrat, Magnetic resonance-guided motorized transcranial ultrasound system for blood-brain barrier permeabilization along arbitrary trajectories in rodents, *J. Ther. Ultrasound.* 3 (2015) 1–11. <https://doi.org/10.1186/s40349-015-0044-5>.
- [28] P.S. Tofts, A.G. Kermode, Measurement of the blood-brain barrier permeability and leakage space using dynamic MR imaging. 1. Fundamental concepts, *Magn. Reson. Med.* 17 (1991) 357–367. <https://doi.org/10.1002/mrm.1910170208>.
- [29] H.B. Mann, D.R. Whitney, On a Test of Whether one of Two Random Variables is Stochastically Larger than the Other, *Ann. Math. Stat.* 18 (1947) 50–60. <https://doi.org/10.1214/aoms/1177730491>.
- [30] J. Seguin, B. Doan, H. Latorre Ossa, L. Jugé, J. Gennisson, M. Tanter, D. Scherman, G.G. Chabot, N. Mignet, Evaluation of Nonradiative Clinical Imaging Techniques for the Longitudinal Assessment of Tumour Growth in Murine CT26 Colon Carcinoma, *Int. J. Mol. Imaging.* 2013 (2013) 1–13. <https://doi.org/10.1155/2013/983534>.
- [31] M.D. Abràmoff, P.J. Magalhães, S.J. Ram, Image Processing with ImageJ, *Biophotoics Int.* (2004).
- [32] R. Di Corato, G. Béalle, J. Kolosnjaj-Tabi, A. Espinosa, O. Clément, A.K.A. Silva, C. Ménager, C. Wilhelm, Combining magnetic hyperthermia and photodynamic therapy for tumor ablation with photoresponsive magnetic liposomes, *ACS Nano.* 9 (2015) 2904–2916. <https://doi.org/10.1021/nn506949t>.
- [33] R. Nallamotheu, G.C. Wood, C.B. Pattillo, R.C. Scott, M.F. Kiani, B.M. Moore, L. a Thoma, A tumor vasculature targeted liposome delivery system for combretastatin A4: Design, characterization, and in vitro evaluation, *AAPS PharmSciTech.* 7 (2006) E7–E16. <https://doi.org/10.1208/pt070232>.
- [34] Y. fei Zhang, J. cheng Wang, D. yan Bian, X. Zhang, Q. Zhang, Targeted delivery of RGD-modified liposomes encapsulating both combretastatin A-4 and doxorubicin for tumor therapy: In vitro and in vivo studies, *Eur. J. Pharm. Biopharm.* 74 (2010) 467–473. <https://doi.org/10.1016/j.ejpb.2010.01.002>.
- [35] H. Jiang, Z.-P. Li, G.-X. Tian, R.-Y. Pan, C.-M. Xu, B. Zhang, J. Wu, Liver-targeted liposomes for codelivery of curcumin and combretastatin A4 phosphate: preparation, characterization, and antitumor effects, *Int. J. Nanomedicine.* Volume 14 (2019) 1789–1804. <https://doi.org/10.2147/IJN.S188971>.
- [36] B. Venegas, W. Zhu, N.B. Haloupek, J. Lee, E. Zellhart, I.P. Sugár, M.F. Kiani, P.L.-G. Chong, Cholesterol Superlattice Modulates CA4P Release from Liposomes and CA4P Cytotoxicity on Mammary Cancer Cells, *Biophys. J.* 102 (2012) 2086–2094. <https://doi.org/10.1016/j.bpj.2012.03.063>.
- [37] V.P. Daswani, U. Ayesa, B. Venegas, P.L.G. Chong, Concentration-induced j-aggregate formation causes a biphasic change in the release of trans-combretastatin A4 disodium phosphate from archaeosomes and the subsequent cytotoxicity on mammary cancer cells, *Mol. Pharm.* 12 (2015) 3724–3734. <https://doi.org/10.1021/acs.molpharmaceut.5b00500>.
- [38] H.D. Do, B.M. Couillaud, B. Doan, Y. Corvis, N. Mignet, Advances on non-invasive physically triggered nucleic acid delivery from nanocarriers, *Adv. Drug Deliv. Rev.* 138 (2019) 3–17. <https://doi.org/10.1016/j.addr.2018.10.006>.
- [39] R. Di Corato, G. Béalle, J. Kolosnjaj-Tabi, A. Espinosa, O. Clément, A.K.A. Silva, C. Ménager, C. Wilhelm, Combining Magnetic Hyperthermia and Photodynamic Therapy

- for Tumor Ablation with Photoresponsive Magnetic Liposomes, *ACS Nano*. 9 (2015) 2904–2916. <https://doi.org/10.1021/nn506949t>.
- [40] D. Needham, G. Anyarambhatla, G. Kong, M.W. Dewhirst, A New Temperature-sensitive Liposome for Use with Mild Hyperthermia : Characterization and Testing in a Human Tumor Xenograft Model, *Cancer Res.* 60 (2000) 1197–1201.
- [41] M. Arthuis, R. Pontikis, G.G. Chabot, J. Seguin, L. Quentin, S. Bourg, L. Morin-Allory, J.C. Florent, Synthesis and structure-activity relationships of constrained heterocyclic analogues of combretastatin A4, *ChemMedChem*. 6 (2011) 1693–1705. <https://doi.org/10.1002/cmdc.201100154>.
- [42] T. Tanaka, S. Shiramoto, M. Miyashita, Y. Fujishima, Y. Kaneo, Tumor targeting based on the effect of enhanced permeability and retention (EPR) and the mechanism of receptor-mediated endocytosis (RME), *Int. J. Pharm.* 277 (2004) 39–61. <https://doi.org/10.1016/j.ijpharm.2003.09.050>.
- [43] D.J. Dark, G.G. Hill, S.A., Prise, V.E., Tozer, G.M., Pettit, G.R., Chaplin, Combretastatin A-4, an agent that displays selective toxicity towards tumour vasculature, *Cancer Res.* 57 (1997) 1829–1834. [https://doi.org/10.1016/S0959-8049\(97\)84574-1](https://doi.org/10.1016/S0959-8049(97)84574-1).
- [44] G.M. Tozer, V.E. Prise, J. Wilson, R.J. Locke, B. Vojnovic, M.R.L. Stratford, M.F. Dennis, D.J. Chaplin, Combretastatin A-4 Phosphate as a Tumor Vascular-Targeting Agent : Early Effects in Tumors and Normal Tissues 1, (1999) 1626–1634.
- [45] L. Nguyen, T. Fifis, C. Malcontenti-Wilson, L.S. Chan, P.N.L. Costa, M. Nikfarjam, V. Muralidharan, C. Christophi, Spatial morphological and molecular differences within solid tumors may contribute to the failure of vascular disruptive agent treatments, *BMC Cancer*. 12 (2012). <https://doi.org/10.1186/1471-2407-12-522>.
- [46] D.W. Siemann, The unique characteristics of tumor vasculature and preclinical evidence for its selective disruption by Tumor-Vascular Disrupting Agents, *Cancer Treat. Rev.* 37 (2011) 63–74. <https://doi.org/10.1016/j.ctrv.2010.05.001>.
- [47] A.C. Fruytier, C.S. Le Duff, C. Po, J. Magat, C. Bouzin, M.A. Neveu, O. Feron, B.F. Jordan, B. Gallez, The blood flow shutdown induced by combretastatin A4 impairs gemcitabine delivery in a mouse hepatocarcinoma, *Front. Pharmacol.* 7 (2016) 1–8. <https://doi.org/10.3389/fphar.2016.00506>.
- [48] T. Vasculature, G. Kong, R.D. Braun, M.W. Dewhirst, Characterization of the Effect of Hyperthermia on Nanoparticle Extravasation from, (2001) 3027–3032.
- [49] S. Dromi, V. Frenkel, A. Luk, B. Traughber, M. Angstadt, M. Bur, J. Poff, J. Xie, S.K. Libutti, K.C.P. Li, B.J. Wood, Pulsed-high intensity focused ultrasound and low temperature - Sensitive liposomes for enhanced targeted drug delivery and antitumor effect, *Clin. Cancer Res.* 13 (2007) 2722–2727. <https://doi.org/10.1158/1078-0432.CCR-06-2443>.
- [50] S.M. Park, M.S. Kim, S.J. Park, E.S. Park, K.S. Choi, Y.S. Kim, H.R. Kim, Novel temperature-triggered liposome with high stability: Formulation, in vitro evaluation, and in vivo study combined with high-intensity focused ultrasound (HIFU), *J. Controlled Release*. 170 (2013) 373–379. <https://doi.org/10.1016/j.jconrel.2013.06.003>.
- [51] A. Kheirrolomoom, C.Y. Lai, S.M. Tam, L.M. Mahakian, E.S. Ingham, K.D. Watson, K.W. Ferrara, Complete regression of local cancer using temperature-sensitive liposomes combined with ultrasound-mediated hyperthermia, *J. Controlled Release*. 172 (2013) 266–273. <https://doi.org/10.1016/j.jconrel.2013.08.019>.
- [52] M. De Smet, E. Heijman, S. Langereis, N.M. Hijnen, H. Grüll, Magnetic resonance imaging of high intensity focused ultrasound mediated drug delivery from temperature-sensitive liposomes: An in vivo proof-of-concept study, *J. Controlled Release*. 150 (2011) 102–110. <https://doi.org/10.1016/j.jconrel.2010.10.036>.
- [53] Z. Abed, J. Beik, S. Khoee, S. Khoei, Original 1, (n.d.) 183–194.

- [54] G. Mauri, L. Nicosia, Z. Xu, S. Di Pietro, L. Monfardini, G. Bonomo, G.M. Varano, F. Prada, P. Della Vigna, F. Orsi, Focused ultrasound: tumour ablation and its potential to enhance immunological therapy to cancer, *Br. J. Radiol.* (2018) 20170641. <https://doi.org/10.1259/bjr.20170641>.